Journal of Physics: Condensed Matter

PAPER

Phonon softening and higher-order anharmonic effect in the superconducting topological insulator $Sr_x Bi_2Se_3$

To cite this article: Mingtao Li *et al* 2020 *J. Phys.: Condens. Matter* **32** 385701

IOP Publishing Journal of Physics: Condensed Matter
J. Phys.: Condens. Matter **32** (2020) 385701 (7pp) https://doi.org/10.1088/1361-648X/ab9344

Phonon softening and higher-order anharmonic effect in the superconducting topological insulator $Sr_xBi_2Se_3$

Mingtao Li[1,6,7], Yifei Fang[2,3,6], Cuiying Pei[4,6], Yanpeng Qi[4] and Lin Wang[1,5,7]

[1] Center for High Pressure Science and Technology Advanced Research, Shanghai 201203, People's Republic of China
[2] Key Laboratory of High Power Laser Materials, Shanghai Institute of Optics and Fine Mechanics, Chinese Academy of Sciences, Shanghai 201800, People's Republic of China
[3] Department of Physics, Fudan University, Shanghai 200433, People's Republic of China
[4] School of Physical Science and Technology, ShanghaiTech University, Shanghai 201210, People's Republic of China
[5] Center for High Pressure Science (CHIPS), State Key Laboratory of Metastable Materials Science and Technology, Yanshan University, Qinhuangdao, Hebei 066004, People's Republic of China

E-mail: linwang@ysu.edu.cn and mingtaoli04@gmail.com

Received 2 March 2020, revised 25 April 2020
Accepted for publication 14 May 2020
Published 19 June 2020

Abstract

We report the anharmonic effect of the Raman-scattering spectrum in the low-carrier density superconductor $Sr_xBi_2Se_3$, which is dominated by the quartic term. Compared to the parent Bi_2Se_3, the superconducting $Sr_xBi_2Se_3$ crystals show obvious phonon softening in the three optical phonon modes A_{1g}^1, E_g^2, and A_{1g}^2. Based on the simulations by the Fano function, we present compelling evidence of the enhanced electron–phonon coupling in $Sr_xBi_2Se_3$ for its smaller asymmetric parameter q. Moreover, an anomalous broadening and intensity antiresonance in the characteristic Raman peaks were observed as the temperature decreased to around 160 K. Thus, the superconducting topological material $Sr_xBi_2Se_3$ represents a counterintuitive example where the electron–phonon interaction is strengthened by the accumulation of electron carriers.

Keywords: anharmonic effect, electron–phonon interaction, topological material

Supplementary material for this article is available online

(Some figures may appear in colour only in the online journal)

1. Introduction

Understanding the superconducting mechanism in doped semiconductors remains controversial and challenging [1–3]. Undoped Bi_2Se_3 is a narrow band layered semiconductor known as a good thermoelectric and topological material [4, 5]. As a representative family of superconducting semiconductors, $Sr_xBi_2Se_3$ is special among (Cu,Sr,Nb)-doped Bi_2Se_3 for having the lowest carrier density ($\sim 10^{19}$ cm^{-3}) while still displaying an observable T_c value at $\sim$3 K [6, 7]. Using angle-resolved photoemission spectroscopy (ARPES) [8], Han *et al* showed that the Sr dopants act as weak electron donors and the topological surface states retains in $Sr_xBi_2Se_3$, compared to the case of Cu and Nb dopants [9–11]. The phonons are believed to be the dominant pairing glue that mediates the superconductivity in doped Bi_2Se_3 [12, 13].

[6] Authors contributed equally to this work.
[7] Author to whom any correspondence should be addressed.

To date, there are only a few experimental reports on how chemical doping affects the lattice dynamics and the electron–phonon interaction (EPI) in doped Bi_2Se_3 superconductors. Using ARPES, Kondo *et al* found two very strong mode couplings in the Dirac-cone surface states at energies of ∼3 and ∼15–20 meV. The mode coupling at ∼3 meV (∼24 cm^{-1}) was further enhanced in the superconducting state of $Cu_xBi_2Se_3$ [14]. Using a neutron scattering experiment, Wang *et al* found that Sr doping can significantly broaden the linewidth of acoustic phonons at small momentum q only along the [001] direction [15], which is attributed to the combined effect of the large and singular EPI as well as the strong Fermi surface nesting [12, 13]. However, the evolution of the optical phonon modes induced by Sr doping remains unclear, which may be relevant to the occurrence of superconductivity in Sr-doped Bi_2Se_3 [3].

Raman-scattering is a powerful and widely adopted tool to investigate the lattice dynamics as well as the electronic excitations in a wide variety of solids such as semiconductors [16–20], and high-T_c superconductors [21–23]. In this work, we report a comparative study of the Raman-scattering spectrum between Bi_2Se_3 and superconducting $Sr_xBi_2Se_3$. We explore the anharmonic effect of the Raman-scattering spectrum in $Sr_xBi_2Se_3$ and present three key observations. First, compared to parent Bi_2Se_3, obvious phonon softening is observed, which can be qualitatively explained by the derived theory for the doped semiconductors [24]. Secondly, enhanced EPI is demonstrated. Lastly, the anharmonic effect is dominated by the quartic term.

2. Experimental methods

Single crystals of Bi_2Se_3 and $Sr_{0.12}Bi_2Se_3$ were grown by the melt method [6]. The source materials were a stoichiometric composition of high-purity metal Sr (2N), Bi (5N), and Se (5N) lumps, which were weighed and loaded into a quartz ampoule. All the operations were completed in an Ar-filled glovebox with oxygen and water levels below 0.1 ppm. The quartz ampoules were evacuated by a vacuum pump and subsequently fused by melting the quartz using a mixed H_2 and O_2 gas flame. The crystal growth was performed by slowly cooling the mixture from 1148 K to 900 K at a rate of 2.5 K h^{-1} in a box furnace. After growth, the crystals were annealed at 900 K for more than 24 h and then quenched.

The magnetic susceptibility measurements were performed on a commercial SQUID-VSM magnetometer down to 1.8 K. The Raman-scattering measurements were performed on the (00l) surface of the same crystal checked by magnetic susceptibility. Before measurements, all the single-crystal samples were freshly cleaved along the c direction and mounted into the chamber of a commercial Linkam stage cryostat equipped with a temperature controller. The samples were cooled down to low temperatures by liquid nitrogen. The Raman-scattering spectra were collected using a Raman microscope spectrometer (Renishaw, UK) with backscattering geometry. A He–Ne laser with a 633 nm wavelength was used as the excitation with 1800-groves/mm grating.

3. Results and discussions

3.1. Crystal structure, Raman modes, and magnetic susceptibility

Sr-doped Bi_2Se_3 crystallizes into a rhombohedral structure ($R\bar{3}m$, no. 166, CN = 6) [9]. The Sr atoms are supposed to be intercalated into the van der Waals gap of Bi_2Se_3 [6, 7], as shown in figure 1(a). In the rhombohedral phase, the Sr, Bi, Se1, and Se2 locate in the Wyckoff sites of 3b, 6c, 3a, and 6c. According to group theory analysis [25, 26], there are four Raman-active modes ($2A_{1g} + 2E_g$) with the even-parity. The schematic of the E_g^1, A_{1g}^1, E_g^2, and A_{1g}^2 modes are shown in figure 1(b). The E_g and A_{1g} modes are related to the shear vibrations between adjacent layers along the *ab* plane and to the vibrations of one layer against the others along the c axis [27], respectively. Figure 1(c) shows the volume magnetic susceptibility versus temperature. The figure 1(c) inset shows that $Sr_{0.12}Bi_2Se_3$ displays a diamagnetic signal at 2.8 K, and the superconducting shielding fraction reaches nearly 80% at 1.8 K, agreeing with reported results [6, 7]. This indicates bulk superconductivity in the experimental $Sr_{0.12}Bi_2Se_3$ crystal. The appearance of superconductivity is believed to be induced by Sr intercalation [6], which can add more electron carriers.

3.2. Raman spectrum and phonon softening

Figures 2(a) and (b) show the Raman-scattering spectrum for Bi_2Se_3 and $Sr_{0.12}Bi_2Se_3$ at different temperatures. Three of the Raman modes are clearly assigned; A_{1g}^1, E_g^2, and A_{1g}^2. The smallest phonon frequency of the E_g^1 mode is out of the detection limit [28], so it is not addressed in this study. To extract the Raman shift and half width at half maximum (HWHM) versus temperature, we fitted the Raman line shape using the Lorentzian function and Fano function [21, 22, 29]:

$$I(\omega) = I_c \frac{(q+\varepsilon)^2}{1+\varepsilon^2} + I_b, \quad (1)$$

where q is the asymmetrical parameter, ε is defined as $\varepsilon = (\omega - \omega_0')/\Gamma$ with the renormalized phonon frequency $\omega_0' = \omega_0 + \Delta\omega_0$, ω_0 is the intrinsic or 'bare' phonon frequency, $\Delta\omega_0$ is the shift value from the ω_0 due to the chemical doping or vacancies, Γ is the HWHM, and I_b is the spectral function of a noninterfering background. Further, the term of I_c can be expressed as [16]: $I_c = \pi\rho(\omega)T_e^2$, where T_e is the Raman matrix element for the connection between the ground state and the excited electronic state, and $\rho(\omega)$ is the joint density of states (DOS) of the electronic continuum. Two representative fitting profiles at 80 K are plotted in figures 2(c) and (d). According to the statistics, the Fano fit is better quality than the Lorentzian fit; see table S1 in the supplementary material (https://stacks.iop.org/JPCM/32/385701/mmedia). In Bi_2Se_3 and $Sr_xBi_2Se_3$, the antiresonance occurs at lower frequency, indicating a positive q value. Note that in the limit of $|q| \to \infty$, the equation (1) recovers to the Lorentzian function [30], $I(\omega) = I_c \frac{1}{1+\varepsilon^2} + I_b$. Actually, the q values range from 40–110, indicating there is little difference between the two

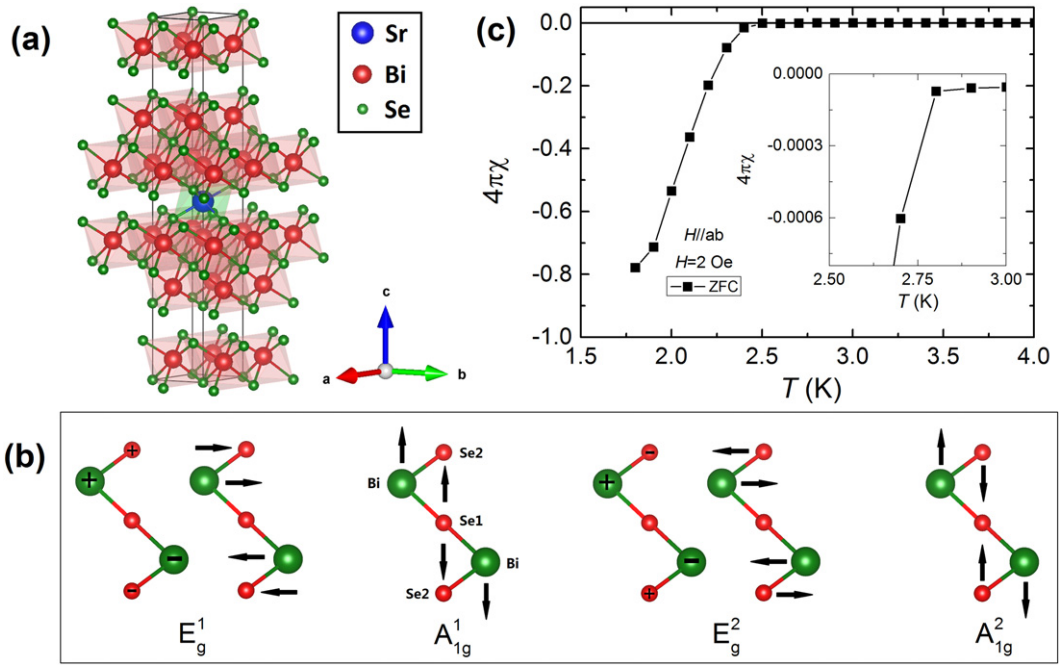

Figure 1. (a) Crystal structure of $Sr_xBi_2Se_3$. (b) Schematic vibrations for the E_g^1, A_{1g}^2, E_g^2, and A_{1g}^1 Raman-active optical modes. (c) Temperature dependence of volume shielding fraction under 2 Oe for single crystal $Sr_{0.12}Bi_2Se_3$ with a magnetic field along the *ab*-plane.

fittings. Moreover, the Fano line shape was also observed in the infrared (IR) active optical modes in Bi_2Se_3 [31].

Figures 3(a), (c) and (e) show the evolution of the Raman frequency versus temperature of Bi_2Se_3 and $Sr_{0.12}Bi_2Se_3$. All three Raman modes manifest a clear phonon softening with respect to Bi_2Se_3. FeSe-based superconductors also experience the phonon softening behavior due to chemical doping or intercalation [23], which accompanies a significant enhancement of the T_c. Considerable softening may also occur when the superconducting transition is crossed, as demonstrated in the high-T_c cuprates [22, 32]. Therefore, the phonon softening due to Sr doping might be a critical element for the emergence of superconductivity in the doped Bi_2Se_3.

With increasing temperature, the Raman frequencies show similar softening behavior, which could be described by the anharmonic process [19, 20]. The temperature dependence of the Raman shift $\omega(T)$ and line width $\Gamma(T)$ is given by: [19, 33]

$$\omega(T) = \omega_0 + \Delta_t^0 + C_\Delta\left(1 + \frac{2}{e^{\hbar\omega_0/2k_BT} - 1}\right) + Q_\Delta\left[1 + \frac{3}{e^{\hbar\omega_0/3k_BT} - 1} + \frac{3}{\left(e^{\hbar\omega_0/3k_BT} - 1\right)^2}\right], \quad (2)$$

$$\Gamma(T) = \Gamma_0 + C_\Gamma\left(1 + \frac{2}{e^{\hbar\omega_0/2k_BT} - 1}\right) + Q_\Gamma\left[1 + \frac{3}{e^{\hbar\omega_0/3k_BT} - 1} + \frac{3}{\left(e^{\hbar\omega_0/3k_BT} - 1\right)^2}\right], \quad (3)$$

where the last three terms of equation (2) represent the anharmonic frequency shift due to thermal expansion Δ_t^0, the cubic Δ_{anh}^c and quartic Δ_{anh}^q contributions, the last two terms of equation (3) represent the line broadening from the cubic Δ_Γ^c and quartic Δ_Γ^q contributions, the C_Δ, C_Γ, Q_Δ, and Q_Γ are fitting constants, and Γ_0 is the temperature-independent contribution that may result from phonon scattering by impurities or the coupling of the phonon to the continuum of the electronic excitations in a normal state for a superconductor [21, 22]. Given the absence of the precise thermal expansion data for both Bi_2Se_3 and $Sr_{0.12}Bi_2Se_3$, an exact treatment including this term is not available at present. Nonetheless, we note the thermal expansion for Bi_2Se_3 has been indirectly extracted from the temperature-dependent XRD patterns [34], which was further adopted to describe the anharmonic effect in Bi_2Se_3 [35]. By fitting the experimental data, we find that using the quartic term in equation (2) alone can already yield a satisfactory description of the softening behavior for $\omega(T)$, as shown by the solid lines in figures 3(a), (c) and (e). In addition, we attempted to describe the $\omega(T)$ including the Δ_t^0 term [34, 35]. Nevertheless, this does not substantially improve the fitting quality, please see tables S2 and S3 in the supplementary material. We conclude that the Raman frequency shifting mainly arises from the four phonons process. Note that previous reports in Bi_2Se_3 show the cubic term is the main contribution describing the anharmonic effect on the $\omega(T)$ and the $\Gamma(T)$ [35, 36], while the quartic term dominates in its counterpart Bi_2Te_3 [36].

The evolution of the $\Gamma(T)$ is displayed in figures 3(b), (d), and (f). We can obtain fairly satisfactory fitting quality when including both the constant contribution term Γ_0 and the quartic term. Since the $Sr_xBi_2Se_3$ material is a weakly electron-doped semiconductor, a vast amount of disorders are supposed

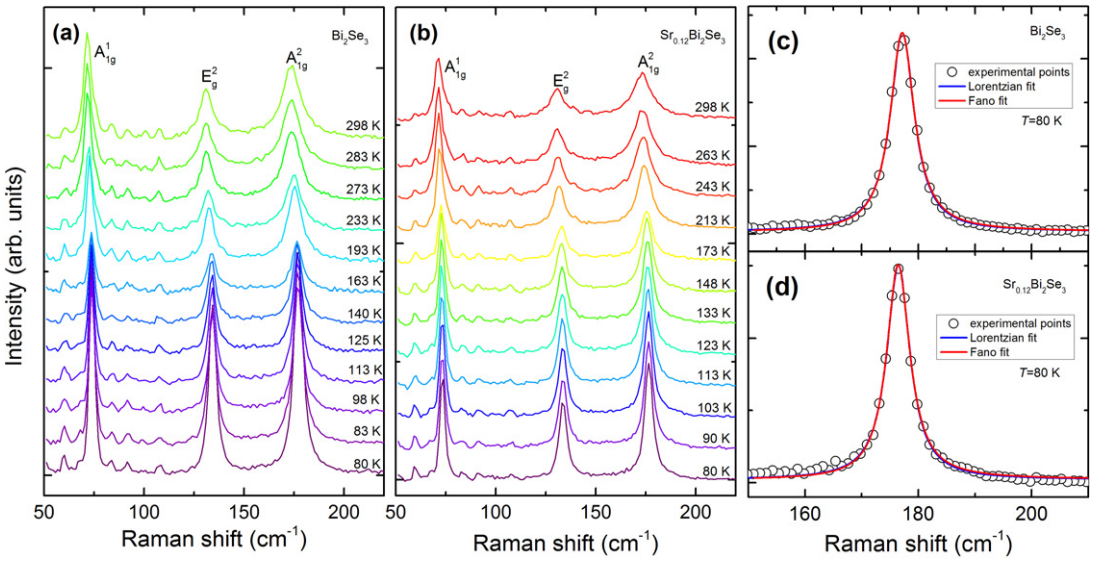

Figure 2. Evolutions of Raman spectrum at different temperatures, and the representative Lorentzian and Fano fitting curves of the A^2_{1g} mode for (a) and (c) Bi_2Se_3, and (b) and (d) $Sr_{0.12}Bi_2Se_3$.

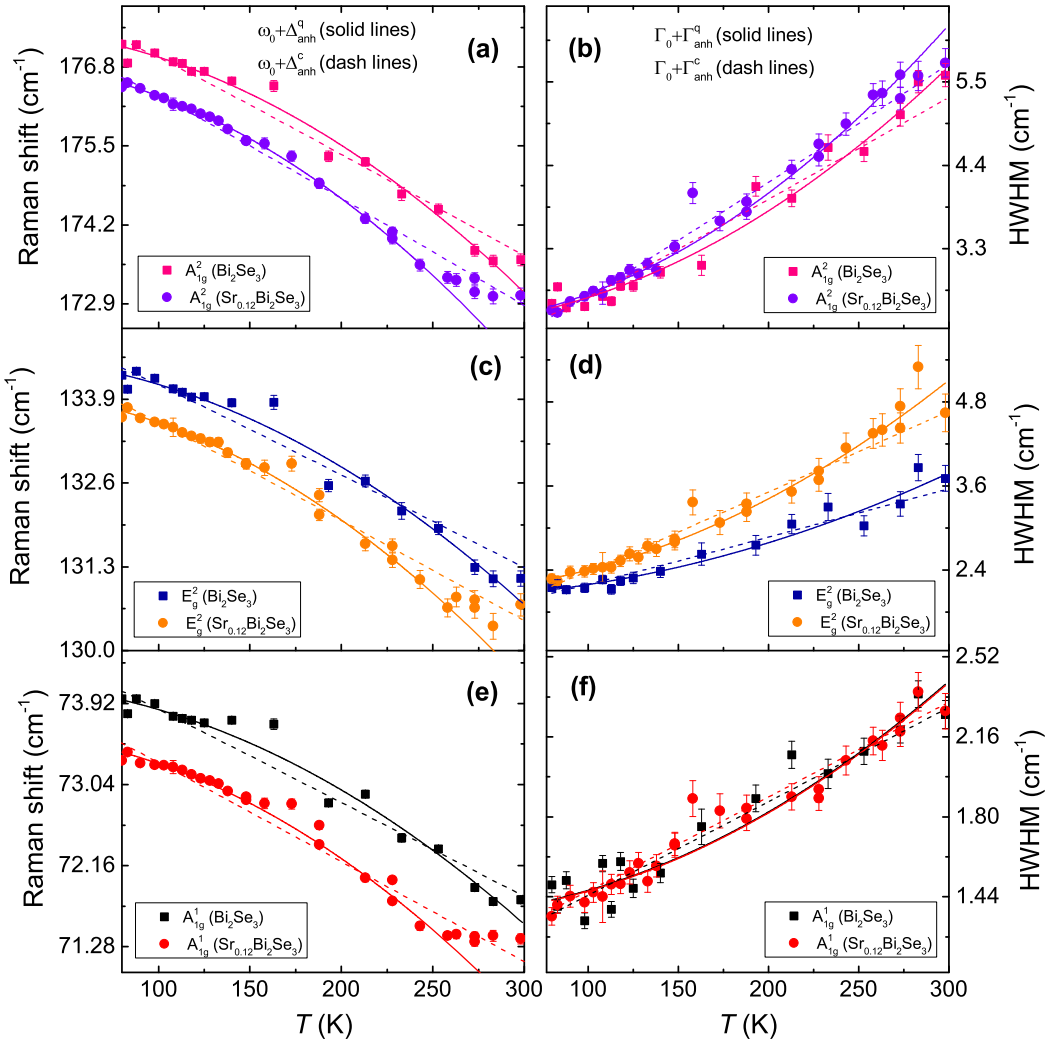

Figure 3. Temperature dependence of the Raman shift and HWHM for the (a) and (b) A^2_{1g} mode, (c) and (d) E^2_g mode, and (e) and (f) A^1_{1g} mode. The solid and dashed lines are the fitting curves from the quartic and cubic contributions, respectively.

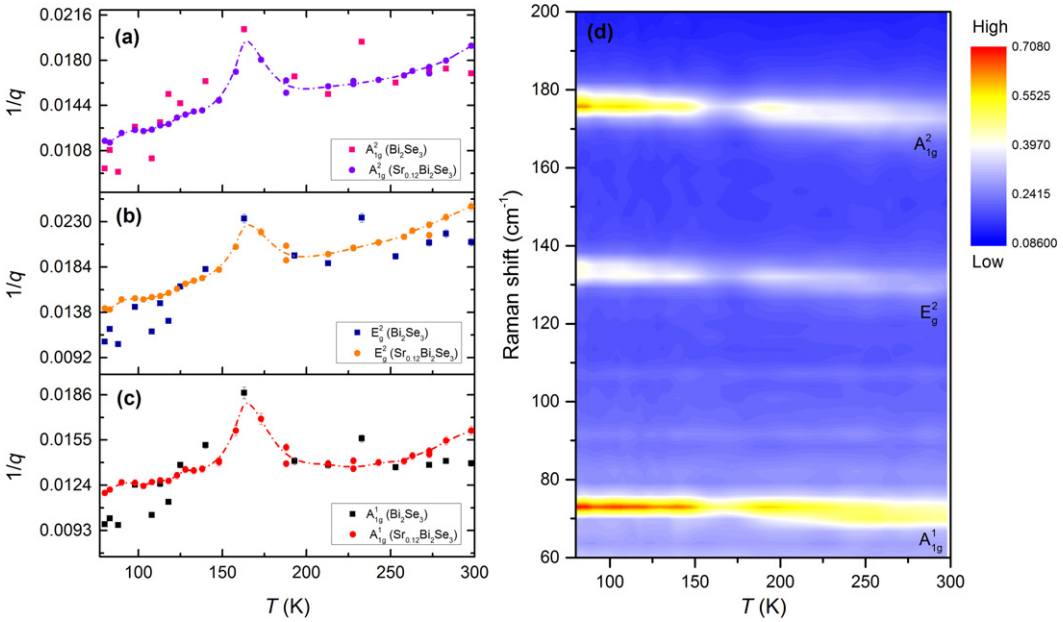

Figure 4. Temperature dependence of $1/q$ for the $Sr_{0.12}Bi_2Se_3$ (a) A^2_{1g} mode, (b) E^2_g mode, (c) A^1_{1g} mode. The dashed dot lines guide the eyes. (d) Intensity evolution of the Raman spectrum. The color represents the distribution of the Raman-scattering intensity.

Table 1. Asymmetry parameters $1/q$ of Bi_2Se_3 and $Sr_{0.12}Bi_2Se_3$ obtained by equation (1).

		ω_{exp} (cm^{-1})		$1/q$	
Sample	Raman mode	80 (K)	298 (K)	80 (K)	298 (K)
Bi_2Se_3	A^1_{1g}	73.97(3)	71.79(4)	0.0097(1)	0.0139(2)
	E^2_g	134.27(4)	131.1(1)	0.01080(7)	0.0209(4)
	A^2_{1g}	177.17(3)	173.6(1)	0.00938(3)	0.0169(1)
$Sr_{0.12}Bi_2Se_3$	A^1_{1g}	73.30(2)	71.36(5)	0.0119(2)	0.0161(3)
	E^2_g	133.62(5)	130.7(2)	0.01420(1)	0.0246(5)
	A^2_{1g}	176.47(3)	173.0(1)	0.01160(7)	0.0191(1)

to reside inside the bulk crystals [37, 38]. This can also be supported by the large residual resistivity and small residual resistivity ratio [6, 7]. The present results indicate that disorders may significantly contribute to scattering the phonons in both Bi_2Se_3 and $Sr_xBi_2Se_3$. Finally, one anomalous feature appears in the $\omega(T)$ and $\Gamma(T)$ data at ~160 K (denoted by T_a) for both Bi_2Se_3 and $Sr_xBi_2Se_3$, where the experimental data points apparently deviate from the theoretical simulation.

3.3. Discussions

To unveil the effect of the Sr doping on the EPI and the origin of the anomalies in the $\omega(T)$ and $\Gamma(T)$, we extracted the q factor in equation (1), as plotted in figures 4(a)–(c). Intriguingly, the inverse of q factor also peaks at $T_a \sim 160$ K. In addition, an obvious reduction of the Raman intensity from 160–180 K is also observed, as plotted in figure 4(d). Recently, similar anomalies have also been reported in Bi_2Se_3 [39], and Sb_2Te_3 [40], and it is proposed that the thermally-activated formation of the stacking faults is responsible for the anomalies in the optical and acoustic phonons, as well as the optical constants. Recently, charge density wave ordering at around 140 K for Bi_2Se_3 and around 220 K for $Cu_xBi_2Te_2Se$ was reported [41, 42]. Also, the magnetic susceptibility study of a superconducting $Cu_xBi_2Se_3$ ($T_c \sim 4.2$ K) crystal revealed a charge density instability at ~96 K [43], somehow lower than that of pure Bi_2Se_3. We suggest that the anomalous deviation of the experimental data points from the theoretical simulation is attributed to the occurrence of the charge density instability since the peaking of the inversed Fano parameter $1/q$ signifies the enhancement of EPI, which may be driven by the lattice instability.

To uncover the electronic response of the anomalies in the $\omega(T)$ and $\Gamma(T)$, we note that the $1/q$ is approximately proportional to the joint DOS $\rho(\omega)$ in $Sr_{0.12}Bi_2Se_3$. To verify this, we took the E^2_g mode as an example for its pronounced shift in the $\Gamma(T)$, reflecting the significant enhancement of the EPI. The q parameter can be expressed as [16]:

$$q = \left[VT_p/T_e + V^2R(\omega)\right] / \left[\pi V^2\rho(\omega)\right], \qquad (4)$$

where T_p is the Raman matrix elements for a one-phonon excited state, V is the anharmonic coefficient describing the EPI matrix element, and $R(\omega)$ is the Raman tensor. Equivalently, the ϵ term in equation (1) can be rewritten as [16]:

$\epsilon = \left[\omega - \omega_0 - V^2R(\omega)\right]/\Gamma$. One can write $\Gamma = \Gamma' + \Gamma''$ where the first term is intrinsic HWHM, and the second is due to the coupling of the excitations continuum [18]. The Raman frequency shift induced by the chemical doping is $\Delta\omega_0 = V^2R(\omega)$, and the line broadening Γ'' is given by $\Gamma'' = \pi V^2\rho(\omega)$. For $Sr_{0.12}Bi_2Se_3$, the frequency shift due to the Sr doping $\Delta\omega_0$ is -0.4 cm^{-1} for the E_g^2 mode at 298 K. Meanwhile, the experimental Γ'' is 0.94 cm^{-1}. With the fitting parameter $q = 40.73$, we obtain $VT_p/T_e = 38.55$. This illustrates that $V^2R(\omega) \ll VT_p/T_e$ truly satisfies, leading to the following relation:

$$1/q \approx (\pi VT_e/T_p)\rho(\omega). \quad (5)$$

As a result, the jumped data points in the $\Gamma(T)$ and Raman spectrum at ~160 K do correlate with the peaks in the $1/q$, i.e., the joint DOS. The experimental ω and the $1/q$ parameters at 80 K and 298 K for Bi_2Se_3 and $Sr_xBi_2Se_3$ crystals are summarized in table 1.

Finally, we discuss the origin of the phonon softening due to the Sr doping and its implications on the occurrence of superconductivity. First, we estimated the carrier relaxation rate $\hbar/\tau$ in $Sr_{0.12}Bi_2Se_3$, which is used to evaluate if the phonon dynamics can be described in the Born–Oppenheimer approximation (BOA) [44]. The BOA requires $\omega\tau \ll 1$ to be satisfied [24]. To make an evaluation, the carrier relaxation lifetime τ can be calculated by $\tau = m^*/n\,\rho_0 e^2$, where m^* is the effective mass in unit of kg, n is the carrier density, ρ_0 is the residual resistivity, and e is the electron charge. Taking $m^* = 0.24m_e$ [7], $n = 2.60 \times 10^{25}$ m^3 at 5 K, and $\rho_0 = 2.32 \times 10^{-6}\,\Omega$ m for $Sr_{0.12}Bi_2Se_3$, we gain $\tau = 1.41 \times 10^{-13}$ s. To obtain the upper bound of the $\omega\tau$, we adopted the fitting frequency of A_{1g}^2 at 0 K, $\omega_0 = 176.97$ cm^{-1}. This yields $\omega_0\tau = 0.75$, which is comparable to the value of unity, implying the system is close to violating the BOA [24, 44]. This situation is usually encountered in the superconducting doped semimetals and semiconductors [3].

Very recently, Sohier *et al* developed an expression for describing the change in the Raman frequencies concerning the neutral semiconducting case [24], which within BOA is given by $\Delta\omega_\nu \approx -N(E_F)\langle g_\nu^2\rangle_{FS}$, where $N(E_F)$ is the DOS at the E_F, and $\langle g_\nu^2\rangle_{FS}$ is the screened square EPI for the νth phonon mode averaged over the Fermi surface. Even when the system obeys $\omega\tau \cong 1$, the phonon softening could still be estimated by [45–47], $\Delta\omega_\nu' \approx \frac{\Delta\omega_\nu}{1+(\omega_\nu\tau)^2}$. Accordingly, phonon softening of $Sr_xBi_2Se_3$ is naturally expected in the phonon modes that are strongly coupled with the electronic states on the Fermi surface. In addition, it is known that the Bi_2Se_3 and $Sr_xBi_2Se_3$ are topological materials hosting surface electronic states, which also potentially couple with optical phonons. However, according to the peaking behavior of $1/q$ at ~160 K, which is related to the bulk charge density instability, it is expected that the bulk electrons on the Fermi surface dominate coupling with the optical phonons. Considering the low-carrier density and thus, low E_F in the $Sr_xBi_2Se_3$ superconductor (for instance, the Fermi temperature $T_F \sim 89$ K can be obtained in 2D limit using effective mass $m^* = 0.24m_e$, which is smaller than the Debye temperature $\Theta_D = 133.3$ K) [7, 48, 49], the traditional BCS theory may be inappropriate for describing its superconductivity. For this reason, the Cooper-pairing scheme for the superconductivity mediated by a strong EPI with the optical phonon modes must be considered [50, 51].

4. Conclusions

In summary, we investigated the anharmonic effect of the Raman frequencies in $Sr_xBi_2Se_3$ single crystals. In contrast to Bi_2Se_3, we observed an obvious phonon softening for the Raman modes in the $Sr_xBi_2Se_3$ superconductor, which can be theoretically explained by the low-energy theory developed by Sohier *et al* [24]. The quartic term dominates the contributions to the shifting of the Raman frequencies and the broadening of the Raman line shape. Interestingly, an anomalous broadening and intensity antiresonance was observed as the temperature decreased to around 160 K. Further, we demonstrated that the electron-phonon interaction is enhanced in the Sr-doped Bi_2Se_3 superconductor. Our findings can facilitate an in-depth understanding of the emerging superconductivity in doped topological insulators with low-carrier density.

Acknowledgments

We appreciate Dr Nana Li and Fengliang Liu for their kind assistance with the set-up for the low-temperature Raman-scattering measurements. We thank Xueyan Du for technical support. This work is mainly supported by the National Natural Science Foundation of China (Grants Nos. 11804011, 11874076, and 11974112), National Science Associated Funding (NSAF, Grant No. U1530402), and Science Challenging Program (Grant No. TZ2016001). Y Q acknowledges funding support from the Science and Technology Commission of Shanghai Municipality (19JC1413900).

ORCID iDs

Mingtao Li https://orcid.org/0000-0003-1594-8008
Yifei Fang https://orcid.org/0000-0001-5702-9005
Cuiying Pei https://orcid.org/0000-0002-2007-6331
Yanpeng Qi https://orcid.org/0000-0003-2722-1375
Lin Wang https://orcid.org/0000-0001-8276-7026

References

[1] Blase X, Bustarret E, Chapelier C, Klein T and Marcenat C 2009 *Nat. Mater.* **8** 375
[2] Bustarret E 2015 *Physica* C **514** 36
[3] Kozii V, Bi Z and Ruhman J 2019 *Phys. Rev.* X **9** 031046
[4] Zhang H, Liu C-X, Qi X-L, Dai X, Fang Z and Zhang S-C 2009 *Nat. Phys.* **5** 438
[5] Heremans J P, Cava R J and Samarth N 2017 *Nat. Rev. Mater.* **2** 17049
[6] Liu Z, Yao X, Shao J, Zuo M, Pi L, Tan S, Zhang C and Zhang Y 2015 *J. Am. Chem. Soc.* **137** 10512
[7] Shruti M V K, Neha P, Srivastava P and Patnaik S 2015 *Phys. Rev.* B **92** 020506
[8] Han C Q *et al* 2015 *Appl. Phys. Lett.* **107** 171602
[9] Hor Y S *et al* 2010 *Phys. Rev. Lett.* **104** 057001
[10] Qiu Y, Sanders K N, Dai J, Medvedeva J E, Wu W, Ghaemi P, Vojta T and Hor Y S 2015 arXiv:1512.03519

[11] Wray L A *et al* 2010 *Nat. Phys.* **6** 855
[12] Wan X and Savrasov S Y 2014 *Nat. Commun.* **5** 4144
[13] Lahoud E *et al* 2013 *Phys. Rev.* B **88** 195107
[14] Kondo T *et al* 2013 *Phys. Rev. Lett.* **110** 217601
[15] Wang J *et al* 2019 *Nat. Commun.* **10** 2802
[16] Klein M V 1983 *Light Scattering in Solids I,* ed M Cardona (Berlin: Springer)
[17] Hart T R, Aggarwal R L and Lax B 1970 *Phys. Rev.* B **1** 638
[18] Chandrasekhar M, Chandrasekhar H R, Grimsditch M and Cardona M 1980 *Phys. Rev.* B **22** 4825
[19] Balkanski M, Wallis R F and Haro E 1983 *Phys. Rev.* B **28** 1928
[20] Menéndez J and Cardona M 1984 *Phys. Rev.* B **29** 2051
[21] Friedl B, Thomsen C and Cardona M 1990 *Phys. Rev. Lett.* **65** 915
[22] Hadjiev V G, Zhou X, Strohm T, Cardona M, Lin Q M and Chu C W 1998 *Phys. Rev.* B **58** 1043
[23] Zhang A, Ma X, Wang Y, Sun S, Lei B, Lei H, Chen X, Wang X, Chen C and Zhang Q 2019 *Phys. Rev.* B **100** 060504
[24] Sohier T, Ponomarev E, Gibertini M, Berger H, Marzari N, Ubrig N and Morpurgo A F 2019 *Phys. Rev.* X **9** 031019
[25] Köhler H and Becker C R 1974 *Phys. Status Solidi* (*b*) **61** 533
[26] Richter W and Becker C R 1977 *Phys. Status Solidi* (*b*) **84** 619
[27] Vilaplana R *et al* 2011 *Phys. Rev.* B **84** 184110
[28] Zhao Y *et al* 2014 *Phys. Rev.* B **90** 245428
[29] Cardona M, Abstreiter G and Pinczuk A 1984 *Light Scattering in Solids IV,* ed M Cardona and G Güntherodt (Berlin: Springer)
[30] Ager J W, Walukiewicz W, McCluskey M, Plano M A and Landstrass M I 1995 *Appl. Phys. Lett.* **66** 616
[31] LaForge A D, Frenzel A, Pursley B C, Lin T, Liu X, Shi J and Basov D N 2010 *Phys. Rev.* B **81** 125120
[32] Bakr M, Schnyder A P, Klam L, Manske D, Lin C T, Keimer B, Cardona M and Ulrich C 2009 *Phys. Rev.* B **80** 064505
[33] Klemens P G 1966 *Phys. Rev.* **148** 845
[34] Chen X *et al* 2011 *Appl. Phys. Lett.* **99** 261912
[35] Kim Y *et al* 2012 *Appl. Phys. Lett.* **100** 071907
[36] Tian Y, Jia S, Cava R J, Zhong R, Schneeloch J, Gu G and Burch K S 2017 *Phys. Rev.* B **95** 094104
[37] Mann C, West D, Miotkowski I, Chen Y P, Zhang S and Shih C-K 2013 *Nat. Commun.* **4** 2277
[38] Du G *et al* 2017 *Nat. Commun.* **8** 14466
[39] Prakash G, Pal K, Waghmare U V and Sood A K 2019 *Phys. Scripta* **94** 115706
[40] Dutta P, Bhoi D, Midya A, Khan N, Mandal P, Shanmukharao Samatham S and Ganesan V 2012 *Appl. Phys. Lett.* **100** 251912
[41] Li Y, Parsons C, Ramakrishna S, Dwivedi A, Schofield M, Reyes A and Guptasarma P 2020 arXiv:2002.12546
[42] Li Y, Smith N P, Rexhausen W, Schofield M A and Guptasarma P 2019 *J. Phys.: Mater.* **3** 015008
[43] Fang Y, You W-L and Li M 2020 *New J. Phys.* **22** 053026
[44] Born M and Oppenheimer R 1927 *Ann. Phys.* **389** 457
[45] Maksimov E G and Shulga S V 1996 *Solid State Commun.* **97** 553
[46] Marsiglio F, Akis R and Carbotte J P 1992 *Phys. Rev.* B **45** 9865
[47] Saitta A M, Lazzeri M, Calandra M and Mauri F 2008 *Phys. Rev. Lett.* **100** 226401
[48] Proust C, Vignolle B, Levallois J, Adachi S and Hussey N E 2016 *Proc. Natl Acad. Sci. USA* **113** 13654
[49] Sun Y, Kittaka S, Sakakibara T, Machida K, Wang J, Wen J, Xing X, Shi Z and Tamegai T 2019 *Phys. Rev. Lett.* **123** 027002
[50] van der Marel D, Barantani F and Rischau C W 2019 *Phys. Rev. Res.* **1** 013003
[51] Gor'kov L P 2016 *Proc. Natl Acad. Sci. USA* **113** 4646